BMC Cancer

RESEARCH

Open Access

Lactate-associated gene MCU promotes the proliferation, migration, and invasion of pancreatic ductal adenocarcinoma

Yuhang Chen[1,2†], Fenglin Zhang[6,7†], Suoyi Dai[1,2†], Jiangang Zhao[4,5], Wenxun Cai[1,2], Ke Zhang[8], Xinghe Liao[2,3*] and Lianyu Chen[1,2*]

Abstract

Background The metabolism of lactate and lactylation of proteins are believed to influence tumor development through their effects on the tumor microenvironment and immune escape mechanisms. Nevertheless, its significance in pancreatic ductal adenocarcinoma (PDAC) has yet to be fully understood. This investigation sought to assess the predictive value and treatment implications of lactate-related genes (LRGs) in PDAC.

Methods We analyzed PDAC data from The Cancer Genome Atlas (TCGA) and Gene Expression Omnibus (GEO), identifying LRGs. Using weighted gene co-expression network analysis (WGCNA) and consensus clustering, we delineated lactate subtypes and extracted differentially expressed genes. Functional enrichment and gene set enrichment analysis (GSEA) analyses were conducted to explore pathways. A lactate-linked risk signature was constructed using Lasso-Cox regression, and its prognostic value was validated. In vitro experiments were executed to examine the function of MCU in PDAC cells. In vitro experiments were conducted to detect the malignant potential of MCU in PDAC cells and its effect on lactic acid metabolism.

Results Two lactate subtypes were identified, with distinct gene expression profiles and clinical outcomes. The risk signature, comprising four LRGs, predicted survival with significant accuracy. In vitro, MCU knockdown reduced cell proliferation, migration, invasion, and stemness, confirming its role in PDAC malignancy. At the same time, it can also inhibit lactate production and glycolysis processes.

Conclusion Our investigation underscores the importance of LRGs in PDAC, providing a novel prognostic signature and therapeutic target.

Keywords Lactate, Pancreatic adenocarcinoma, Tumor microenvironment, Prognosis, MCU

†Yuhang Chen, Fenglin Zhang and Suoyi Dai contributed equally to this work.

*Correspondence:
Xinghe Liao
fdzlxinghe@163.com
Lianyu Chen
lianyu-chen@hotmail.com

Full list of author information is available at the end of the article

Introduction

Pancreatic ductal adenocarcinoma (PDAC) constitutes an exceptionally deadly type of malignancy [1]. It is anticipated that by the year 2030, PDAC will ascend to become the second most prevalent cause of cancer mortality in the United States [2]. The incidence of PDAC is increasing. However, the 5-year survival rate remains around 13% despite advanced treatments, including surgery, radiation therapy, immunotherapy, and targeted therapy.

[3, 4]. *Despite extensive research into its biology and pathophysiology, it may still seem inadequate*, applying this understanding in clinical settings to enhance patient outcomes remains a significant challenge [5]. Hence, identifying key genes that could potentially govern the initiation and progression of PDAC is of paramount importance, as they may offer new avenues for therapeutic intervention.

Lactate, once regarded merely as a metabolic byproduct of anaerobic glycolysis, has emerged as an essential factor in the development of malignant tumors, including PDAC. The Warburg effect, characterized by a preference for glycolysis over oxidative phosphorylation, results in elevated lactate production within the tumor microenvironment (TME) [6]. The buildup of this metabolite leads to TME acidification, which has profound implications for tumor biology. The resulting acidic conditions diminish immune cell effectiveness, particularly T lymphocytes and natural killer cells, through suppression of their cytotoxic activities and growth [7]. Moreover, investigations have demonstrated that lactic acid drives macrophage transformation toward an immunosuppressive M2 state, thereby suppressing anti-tumor immune responses [8]. Lactate also acts as a signaling molecule, influencing tumor cell behavior by regulating various signaling pathways, such as the GPR81 pathway, which modulates immune evasion and tumor growth [9]. In PDAC, lactate serves a crucial function in metabolic reprogramming, supporting tumor cell survival and proliferation by providing essential carbon skeletons for biosynthesis [10]. Furthermore, lactate can affect tumor angiogenesis by stabilizing hypoxia-inducible factors (HIFs) and promoting the expression of angiogenic factors [11]. The multifaceted effects of lactate on the TME highlight its significance as a target for therapeutic intervention in pancreatic cancer, offering potential avenues for improving treatment outcomes [12, 13].

In this study, aiming to reveal the intricate interactions between *Lactate-related genes (LRGs)* and PDAC prognosis, we utilized transcriptomic and single-cell data obtained from public databases to establish a predictive survival model for PDAC. By integrating bioinformatics techniques, we found that MCU was closely associated with the prognosis of PDAC. Finally we validated the potential relationship between MCU and PDAC and its significance in the progression of PDAC using multiple experimental approaches.

Materials and methods

Datasets

The Cancer Genome Atlas (TCGA) is a public project cataloging key genomic changes in cancer. We analyzed PDAC data (https://portal.gdc.cancer.gov/) from TCGA, excluding cases with 0 survival time, *perioperative deaths and cases with missing data*, resulting in 176 tumors and 4 normal tissue samples. A prognostic validation dataset, GSE62452, was procured from GEO (https://www.ncbi.nlm.nih.gov/geo/).

From GeneCards (http://www.genecards.org), we identified 2208 Lactate-related genes (LRGs). A set of 206 LRGs were retrieved from the prior literature [14]. After removing the duplicated genes, we got a total of 2346 LRGs, detailed in Supplementary Table 1.

WGCNA and Pinpointing the differentially expressed genes (DEGs)

The gene co-expression network within the TCGA-PAAD dataset was generated utilizing the "WGCNA" package. The essential module was identified as having both the maximum Pearson coefficient and the strongest link to clinical characteristics. Modules were established using average linkage hierarchical clustering based on topological overlap matrix (TOM) dissimilarity, followed by dynamic tree-cutting with a minimum module size of 30 genes, and merged if eigengene dissimilarity was < 0.25.

Statistical analysis of mRNA expression across diverse cohorts was executed utilizing the t.test function in R software. Subsequently, the p.adjust function was employed to determine a marked False Discovery Rate (FDR) for individual genes, which facilitated the extraction of differential expression profiles. The mRNAs were screened for differential expression based on the following criteria: an adjusted P-value below 0.05 and an absolute fold change exceeding 1.5.

Consensus clustering

This study utilized the ConsensusClusterPlus package in R to perform consensus clustering, aiming to uncover molecular subgroups associated with Lactate. The ideal number of subtypes, k, was determined using the consensus matrix, consensus score, and cumulative distribution function (CDF) cure. To validate the findings, the optimal cluster count was evaluated for values of k ranging from 2 to 10, with the entire procedure iterated 1000 times for robustness. Cluster visualizations were produced utilizing the Pheatmap package in R.

Functional enrichment analysis of the data

The KEGG REST API was employed for pathway analysis (https://www.kegg.jp/kegg/rest/keggapi.html). We conducted an enrichment evaluation on recent KEGG pathway gene classifications employing the R package clusterProfiler. Gene collections were screened with a lower threshold of 5 genes and an upper limit of 5000. Statistical relevance was ascertained by $P < 0.05$ and FDR < 0.1. For gene collection enrichment, we implemented the GO annotations from the R package org.Hs.eg.db and aligned genes to background collections using clusterProfiler for enrichment examination.

Gene set enrichment analysis (GSEA) of the data

GSEA scores were sourced from the Broad Institute's database (http://www.gsea-msigdb.org/gsea/downloads.jsp). We combined the low and high Immunosenescence cohorts and applied GSEA v3.0 to the C2.cp.kegg.v7.4 gene set. We used GMT subset analysis with parameters set for 5000 gene set size, 1000 permutations, and a minimum of 5 genes. Significance was established at $P < 0.05$ and FDR < 0.1.

Survival analysis

Cluster associations with overall survival (OS) were examined utilizing the R package 'survival'. Outcomes were visualized with heat maps from 'pheatmap' and Kaplan-Meier (KM) curves from 'survminer'.

Constructing the lactate-linked risk signature

To avoid overftting, the least absolute shrinkage and selection operator (LASSO) was used to select genes with high prognostic values. Next, 1000 LASSO iterations were performed using the 'glmnet' package in R to construct the prognostic models and obtain their regression coefcients, and the model was optimized through 10-fold cross-validation.

Examination of immune landscape between 2 lactate subgroups

Each sample's immune cell score was computed utilizing the R package IOBR, which applies the Cibersort and Estimate algorithms to expression data. IOBR serves as a standard computational tool for analyzing immune-tumor interactions.

Expression verification of LRGs

We examined the mRNA expression differences in PDAC tissues utilizing the GEPIA2 platform (http://gepia2.cancerpku.cn/#index), which consolidates information from both TCGA and GTEx databases.

Single cell analysis

The LRG expressions within the immune cells were examined at the single-cell level using the Tumor Immune Single Cell Center (TISCH) database (http://tisch.comp-genomics. org/).

Cells and treatments

The pancreatic cancer cell lines Bxpc3 and Capan1 were procured from the American Type Culture Collection (ATCC, USA). For Capan1 cells, cultivation was performed in Dulbecco's modified Eagle's medium (DMEM, Cat. C11995500BT, Gibco, USA) enriched with fetal bovine serum (FBS, Cat. 10099–141 C, Gibco, USA, 10%), penicillin (100 U ml^{-1}), and streptomycin (100 mg ml^{-1}) (Cat. 15140-122, Gibco, USA). For Bxpc3 cells, cultivation was conducted in RPMI-1640 (Roswell Park Memorial Institute medium 1640, Cat. 11875093, Gibco, USA) enriched with FBS (Cat. 10099–141 C, Gibco, USA, 10%), penicillin (100 U ml^{-1}), and streptomycin (100 mg ml^{-1}) (Cat. 15140-122, Gibco, USA). Cell cultivation was sustained in a moisture-controlled setting at 37 °C with 5% CO2 utilizing a Thermo Scientific HERACELL 240i CO2 Incubator (240i, Thermo Scientific, USA). In subsequent experiments, the cells were counted using a cell counter to ensure that the number of cells was accurate, three technical replicates were performed per sample to ensure accuracy.

qRT-PCR

1 mL of RNAiso Plus reagent (Takara,9109, China) was introduced to the cells. Following complete mixing and centrifugation, the upper liquid phase was removed. The total RNA precipitate underwent purification with 75% ethanol solution, subsequently yielding RNAs for reverse transcription. The detailed protocol was executed in accordance with the guidelines of PrimeScript™ RT Master Mix (Takara, RR036A China) and TB Green® Premix Ex Taq™ II (Takara, RR820A, China). The annealing temperature of the PCR amplification program is 95° and the number of cycles is 40. The real-time PCR analysis was conducted following the operational protocols of the 7500 Real-Time PCR System (Takara, RR820A China). The quantification of gene expression at the mRNA level was determined using the $2^{-\Delta\Delta Ct}$ methodology, with final values standardized against β-actin expression. The MCU primer sequences were: AGGATCGGGGAATTGACAGAG (F), GTGTGGTGTATAGTTGCTGGAC (R); The sequence of β-actin primers: CGTGCGTGACATTAAGGAGAA (F), AGGAAGGAAGGCTGGAAGAG (R);

Cell transfection

Cells were placed on 6-well plates at 0.8×10^6 cells/well and maintained overnight in a 37 °C incubator containing 5% CO2 until reaching approximately 70% confluence for

DNA transfection. Per the supplier's protocols, 2.5 μg/well plasmid was introduced into the cells using Lipofectamine 3000 (Thermo Fisher Scientific, L3000015; USA).

Western blot

The immunoblotting assay was executed per the standard protocols outlined in earlier studies. In brief, cells underwent lysis utilizing Radio Immunoprecipitation Assay Lysis buffer (Cat. 87787, Thermo Scientific, USA, RIPA) comprising protease (Cat. 04693124001, Roche, Switzerland) and phosphatase inhibitors (Cat. B15001-A, Bimake, USA) for 30 min on ice. After centrifugation (12500 rpm for 15 min at 4 °C), we obtained the supernatant. Equal amounts of total proteins were then separated through 10% SDS-polyacrylamide gel electrophoresis. The protein components were subsequently transferred to a polyvinylidene difluoride membrane (0.45 μm, Millipore, Billerica, MA). Following blockage with 5% BSA (Cat. SLBN9354V, Sigma-Aldrich, USA), the membrane underwent incubation with primary antibodies targeting these proteins at specified dilutions: MCU(1:2000, A22525, Abclonal, China), GLUT1 (1:2000, 21829-1-AP, proteintech, China), HIF-1 A (1:2000, 9321, GenuIN biotech, USA), HK2 (1:5000, 22029-1-AP, proteintech, China), LDHA (1:5000, 19987-1-AP, proteintech, China), PDK (1:1000, 10026-1-AP, proteintech, China), PFKFB3 (1:2000, 13763-1-AP, proteintech, China), PKM2 (1:5000, 60268-1-Ig, proteintech, China), p-PDHA (1:2000, 29582-1-AP, proteintech, China), β-actin(1:2000, 4967 S, Cell Signaling Technology (CST), USA). The samples were maintained at 4 °C overnight, followed by treatment with a horseradish peroxidase-conjugated goat anti-rabbit IgG (H + L) antibody. The membranes were then exposed to HRP Substrate (Millipore Corporation, Billerica, MA, USA) for visualization, and signal detection was accomplished utilizing a Bio-Rad ChemiDoc MP System (ChemiDoc MP, Bio-Rad, USA). The Western Blot band signal was quantitatively analyzed by ImageJ software. First, the background noise was deducted, and then the gray value of the target protein was standardized with the gray value of β-actin.

Cell proliferation assays in vitro

For the CCK-8 analysis, cells were distributed into 96-well plates with 2×10^3 cells in each well. After that, the Cell Counting Kit-8 (CCK8) solution (DOJINDO, CK04, Japan) was introduced, and the microplates were kept in darkness for 2 h. The absorbance readings were then obtained at 450 nm wavelength. Regarding the colony-formation experiment, cells were initially plated at 500 cells per well and cultured in a 6-well cell culture plate (Corning) for 15 days. The cells were then stabilized with 4% paraformaldehyde and colored utilizing 0.2% crystal violet (Sigma). Using ImageJ software, we counted colonies containing over 50 cells, the threshold is set from 0 to155, the particales is set from 50 to 1000.

Sphere formation assay

Cells were grown in DMEM medium containing insulin (4 ng/mL; Sigma), basic fibroblast growth factor (10 ng/mL; Sigma), EGF (100 ng/mL; Sigma), and B-27 (2%; Invitrogen) was undertaken in an ultra-low attachment 6-well plate (Costar). Renewal of the medium was conducted every 2–3 days. Ten days later, spheroids were visualized using a microscope (Nikon).

Migration assay

To evaluate the cell invasion potential, cells in culture were diluted to 2×10^5 cells/mL within the serum-free medium, and 200 μL of this cellular preparation was introduced to the upper portion of the transwell chamber (8.0 μm pore size, No. 3422; Corning, USA). The lower compartment received 800μL of medium containing 10% FBS. Following a twenty-four hour incubation period, cells remaining on the upper surface were carefully eliminated using a cotton swab moistened with ice-cold PBS. Subsequently, cells that had migrated to the basolateral membrane were stabilized using 4% PFA (Sigma-Aldrich) for 30 min, succeeded by crystal violet (Sigma-Aldrich) staining conducted over 2 h at ambient temperature.

Invasion assay

Using serum-free medium on ice, the matrix glue was diluted at a ratio of about 1:8, added to the upper chamber at a rate of 100μL/ well, spread over the bottom of the chamber, and incubated in the cell incubator for 2 h. The excess matrix glue liquid in the upper chamber was gently sucked out, 200μL of cell suspension with serum-free medium was added, and 800μL of complete medium was introduced to the lower compartment. When returning to the chamber, be careful not to generate bubbles. After twenty-four hours of cell placement, the cells on the upper compartment surface were delicately eliminated utilizing a cotton applicator with ice-cold PBS. Cells adhering to the basolateral membrane of the compartment insert were subsequently stabilized with 4% PFA (Sigma-Aldrich) for 30 min, succeeded by crystal violet (Sigma-Aldrich) staining for 2 h at ambient temperature.

Determination of lactic acid content

The lactate concentration was measured using the L-lactate Dehydrogenase Detection Kit (WST-8 Method) (Beyotime, P0393S, China) in accordance with the manufacturer's protocol.

Determination of NAD+, NADH and NAD+/NADH

The NAD+/NADH Detection Kit (WST-8 Method) (Beyotime, S0175, China) was used for measurement in accordance with the manufacturer's protocol.

Statistical analyses

Statistical analysis was executed utilizing R (v4.4.1), implementing KM survival assessment and the log-rank method for survival comparisons. A significance level of $P < 0.05$ was adopted for statistical computations. GraphPad Prism v. 9.01 (GraphPad Software) was employed for data analysis. Data normality was assessed using the Shapiro-Wilk test ($\alpha = 0.05$) applied to model residuals. Homogeneity of variances across experimental groups was verified through Levene's test ($\alpha = 0.05$). For datasets violating normality assumptions, appropriate nonparametric alternatives or data transformations were employed. All statistical analyses were conducted using R 4.3.1, with graphical validation via Q-Q plots and residual scatterplots. Comparison between the two groups: student t test (unpaired, two-tailed) was used. For comparisons involving three or more groups: one-way ANOVA and Tukey post hoc tests were used to control for multiple comparisons. The parameters were assessed by the χ2 test or Fisher precision test, and the classification parameters were tested using the student t test for paired samples. Adjustment of multiple tests: Bonferroni correction when appropriate. The homogeneity of variance was confirmed by Levene test. A p value < 0.05 is considered significant, and the significance level is indicated by an asterisk (*:$p < 0.05$; **:$p < 0.01$, ***:$p < 0.001$, ****:$p < 0.0001$). The findings are denoted as means ± SEM derived from three autonomous experiments, each conducted in duplicate. Each experiment included three technical and biological replicates for quantitative assays. Data are presented as mean ± SD.

Results

Consensus clustering for lactate subtype identification and DEGs pathway analysis

The "limma" program was utilized to detect 1740 DEGs between PDAC and normal tissues (Fig. 1A). Subsequently, the 30 DEGs with the highest significance of differences are shown in Fig. 1B. To obtain hub genes in individuals with PDAC, we examined candidates by WGCNA analysis. Utilizing the hierarchical clustering approach, the co-expressed genes were categorized into distinct modules and assigned color codes (Fig. 1C). We then investigated the link between modules and individuals with PDAC and generated the module-trait heatmap using Spearman's correlation analysis (Fig. 1D). We then found 24 intersecting genes (Fig. 1E). The expression levels of these 24 LRGs exhibited significant variation between the normal tissues and PDAC samples, as illustrated in Fig. 1F.

Subsequently, employing consensus clustering, two clusters of PDAC associated with lactate were delineated. Utilizing the TCGA dataset, these two clusters demonstrated distinct lactate gene expression profiles following k-means clustering analysis, as depicted in Fig. 2A-B. The expression of LRGs was low in cluster C1 and high in cluster C2 (Fig. 2C). Furthermore, survival analysis suggested that these lactate-derived subgroups exhibited markedly distinct clinical outcomes. Notably, the C2 subgroup exhibited a better survival rate compared to the C1 subgroup, as illustrated in Fig. 2D.

Identifying the DEGs and signal pathways in the various lactate subcategories

Within this investigation, essential DEGs and crucial signaling pathways from both classifications were examined to elucidate the molecular mechanisms influencing prognosis across the two lactate subgroups. Analysis revealed 2055 differentially expressed genes (Fig. 3A). These genes were found to be enriched in functions of the immune system, encompassing cell adhesion molecules (CAMs), chemokine signaling pathways, hematopoietic cell lineage, Pancreatic secretion, Th17 cell differentiation, extracellular region, immune system process, immune response, cell motility, and regulation of immune system process, as represented in Fig. 3B-C. The observations suggested that genes associated with Lactate demonstrated connections to the immune microenvironment. Comparative analysis between C1 and C2 subcategories utilized the GSEA methodology. Through GSEA-KEGG analysis, we found that cluster C1 was significantly enriched in base excision repair, steroid biosynthesis, and terpenoid backbone biosynthesis pathways, while cluster C2 showed significant enrichment in autoimmune thyroid disease, chemokine signaling pathway, and calcium signaling pathway (Fig. 3D). Through GSEA-GO analysis, we demonstrated that cluster C1 was significantly enriched in brush border assembly, spindle elongation, and positive regulation of spindle assembly, whereas cluster C2 exhibited prominent enrichment in cyclic nucleotide biosynthetic process, phagolysosome assembly, and G protein-coupled receptor signaling pathway (Fig. 3E).

Somatic mutations and the TME in diverse immunosenescence risk cohorts

The analysis uncovered that unique somatic mutation patterns existed between the two subtypes (Fig. 4A). The genes exhibiting the highest mutation frequencies included KRAS, TP53, SMAD4, CDKN2A, TTN, and MUC16. In this analysis, we explored the disparities in the TME across two distinct patient cohorts. Figure 4B presents a comprehensive overview of the immune cell

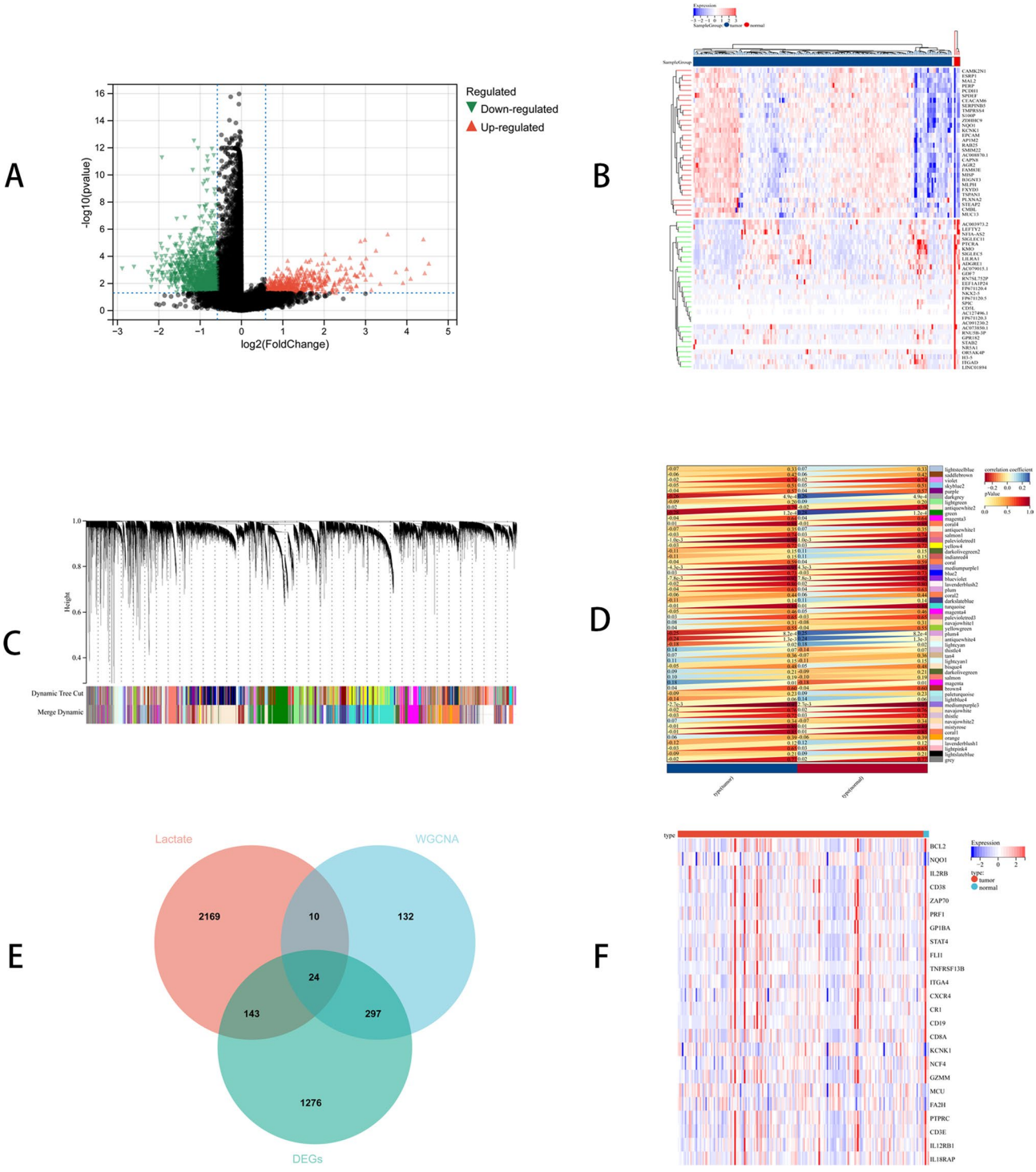

Fig. 1 Analysis and visualization of differentially expressed genes. (**A**) Expression patterns of DEGs comparing PDAC versus normal tissues; (**B**) Leading 30 DEGs identified between PDAC and control samples. Selection of central genes through WGCNA; (**C**) Hierarchical clustering tree; (**D**) Heat visualization of module-trait associations; (**E**) Overlapping analysis depicting shared genes among LRGs, module-specific genes and DEGs; (**F**) Expression profile matrix showing 24 LRGs across PDAC and adjacent normal specimens from the TCGA dataset

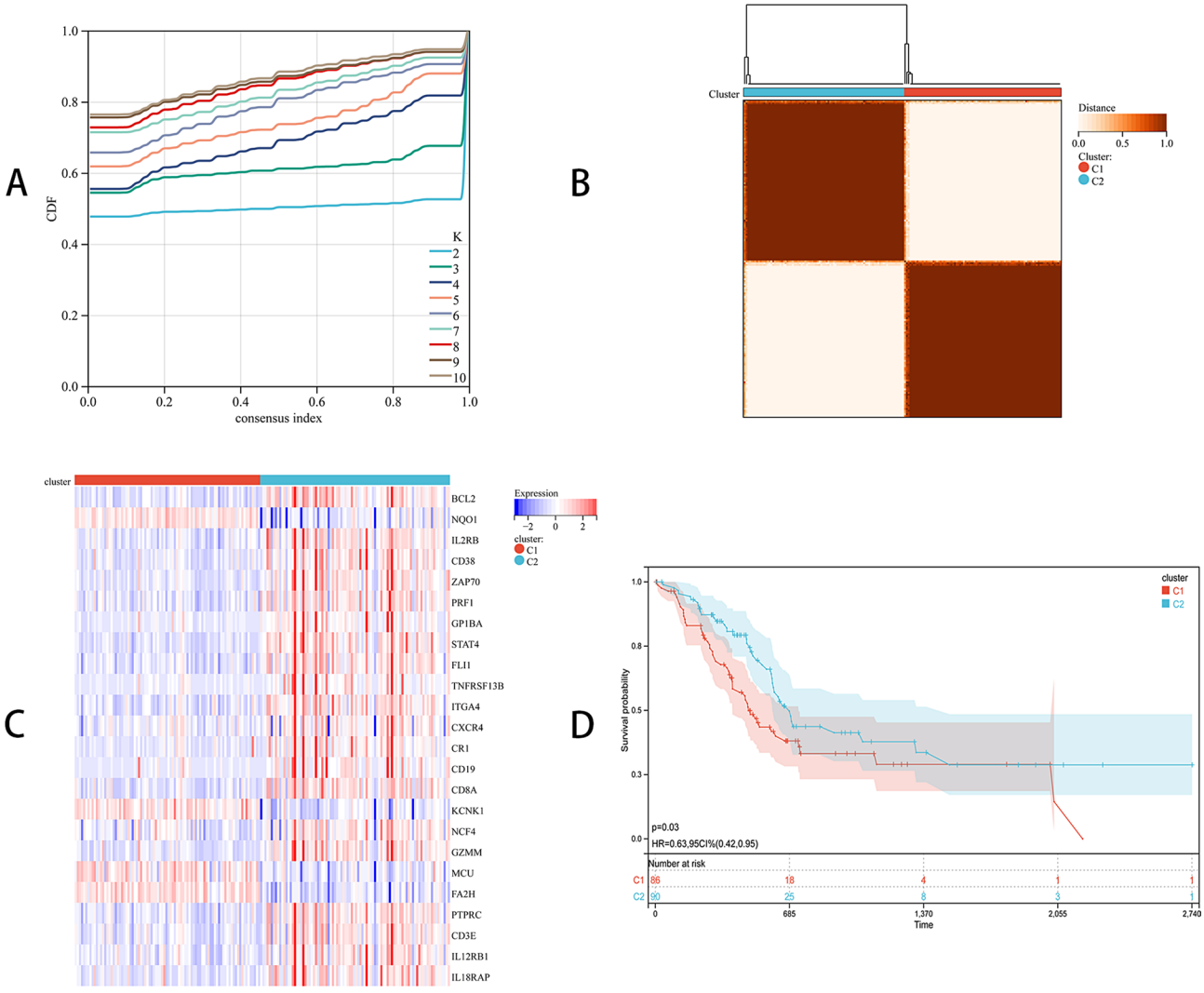

Fig. 2 Identification of Lactate-associated subgroups through consensus clustering. (**A**)The delta area curve for consensus clustering illustrates the comparative differences in the area beneath the cumulative distribution function (CDF) curve for k values ranging from 2 to 10; (**B**) The consensus pattern of the clustering examination utilizing k-means clustering (k = 2); (**C**) The expression patterns of 24 LRGs are displayed in the heatmap visualization; (**D**) KM plots showing patient OS between the C1 and C2 subgroups

infiltration patterns among 176 PDAC patients, as documented in the TCGA dataset. Employing the Cibersort algorithm and the lm22 gene signature matrix, we assessed the presence of 22 distinct immune cell types in each cohort.

Our findings revealed that the C2 cohort demonstrated superior immune activity, as evidenced by higher ImmuneScore, StromalScore, and EstimateScore, indicating a more robust immune response within the TME individuals(Fig. 4C). Furthermore, the C1 cohort displayed a notable reduction in the prevalence of naive B cells, memory B cells, CD8 + T cells, activated CD4 + T cell memory, and activated NK cells, as opposed to those in the C2 cohort. Conversely, the C1 cohort demonstrated increased levels of plasma cells, M0 macrophages, monocytes and eosinophils (Fig. 4D). These observations highlight the complex interactions among immune cell dynamics and the risk stratification of PDAC patients.

Establishment and validation of the lactate risk signature

In this study, we have developed an innovative prognostic model predicated on the LRGs. The Lasso regression analysis was employed to assess these three LRGs, and they were consequently selected to form the predictive model, as illustrated in Fig. 5A-B. By setting the lambda value at 0.06676, we were able to pinpoint three key genes. The predictive model is encapsulated in the following formula: Riskscore = (0.00199 * NQO1) - (0.09731 * STAT4) + (0.15009 * KCNK1) + (0.05063 * MCU).

Utilizing the median risk score, we categorized our study population into a high-risk cohort (H) and a low-risk cohort (L). We utilized the TCGA dataset as our

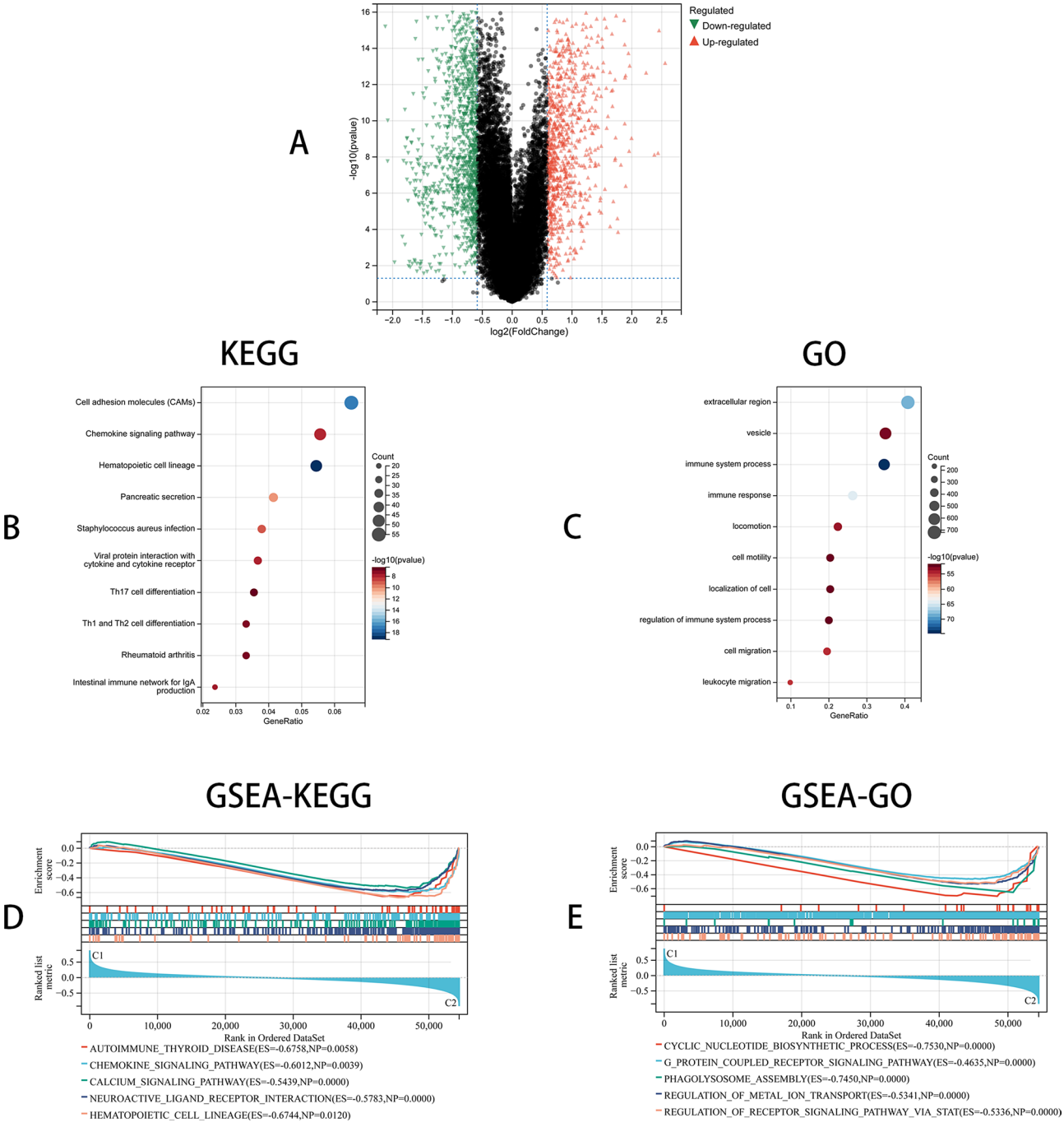

Fig. 3 Identification of DEGs and related signaling pathways. (**A**) DEG distribution between C1 and C2 subgroups within TCGA dataset; (**B**-**C**) Pathway enrichment analyses using KEGG and GO. (**D**-**E**) GSEA identifies key signal pathways present in both subcategories

training cohort and the GSE62452 dataset as the validation cohort. Furthermore, the connection between the two cohorts and OS status was evaluated. The findings revealed that a markedly lower proportion of patients in the H cohort survived in the TCGA dataset, with a more pronounced effect in the H cohort (Fig. 5C). The KM survival assessment corroborated that individuals in the H cohort experienced shorter survival times compared to those in the L cohort, as evidenced in both two cohorts (Fig. 5D and F). In the training cohort, the receiver operating characteristic (ROC) curves were developed with area under the curve (AUC) values of 0.56 for the 1-year survival, 0.58 for the 3-year survival, and 0.64 for the 5-year survival (Fig. 5E). Similarly, in the validation cohort, the ROC curves were generated with AUC values

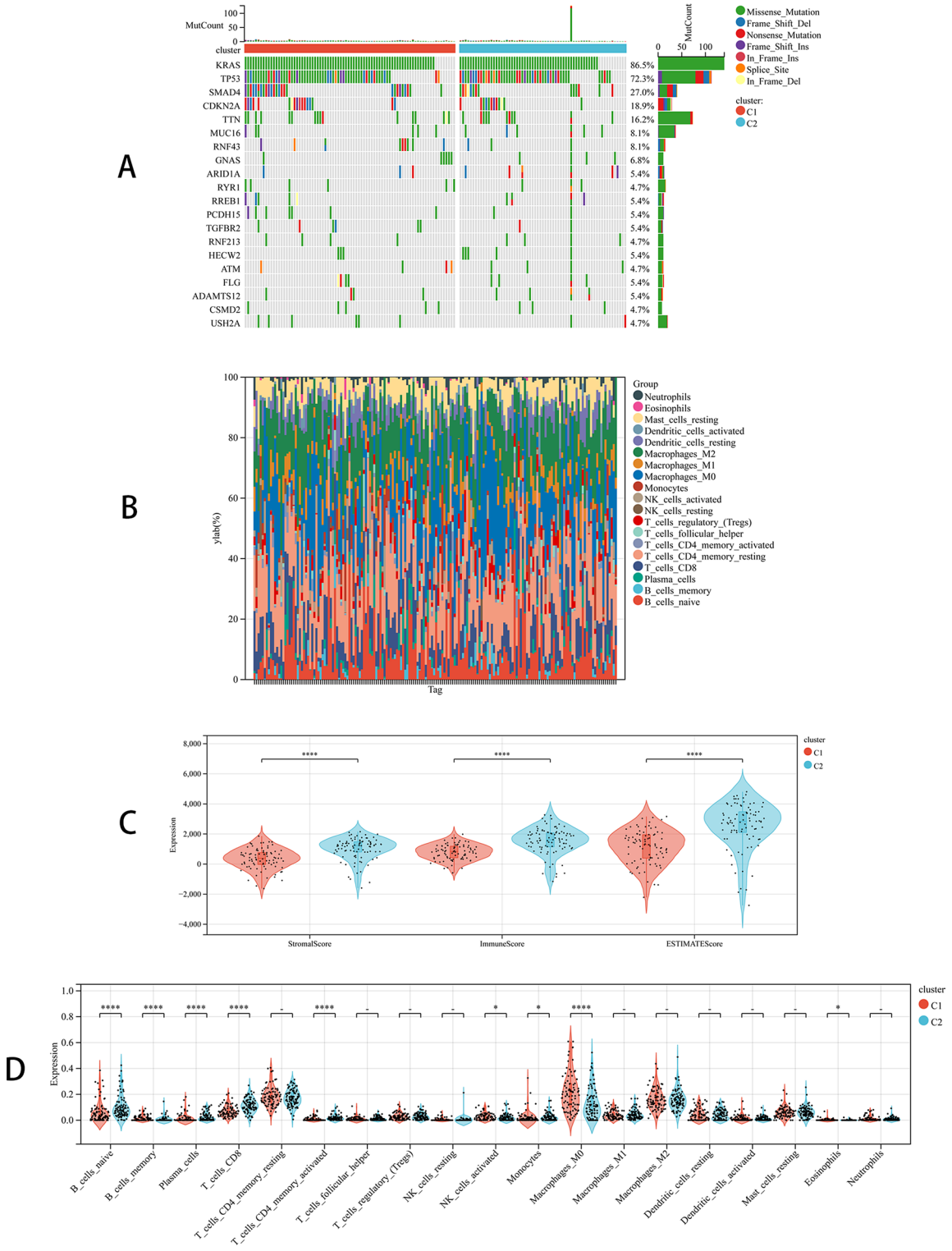

Fig. 4 Immunological characteristics of distinct Lactate subcategories. (**A**) Assessment of somatic mutation patterns among Lactate classifications. (**B**) Comparative distribution of immune cell infiltration; (**C**) Stromal, Immune, and Estimate scores for two subcategories (Independent *t-test*); (**D**) Notable disparities in immune cell infiltration between subcategories (Independent *t-test*). (* $P<0.05$;** $P<0.01$;*** $P<0.001$;****$P<0.0001$)

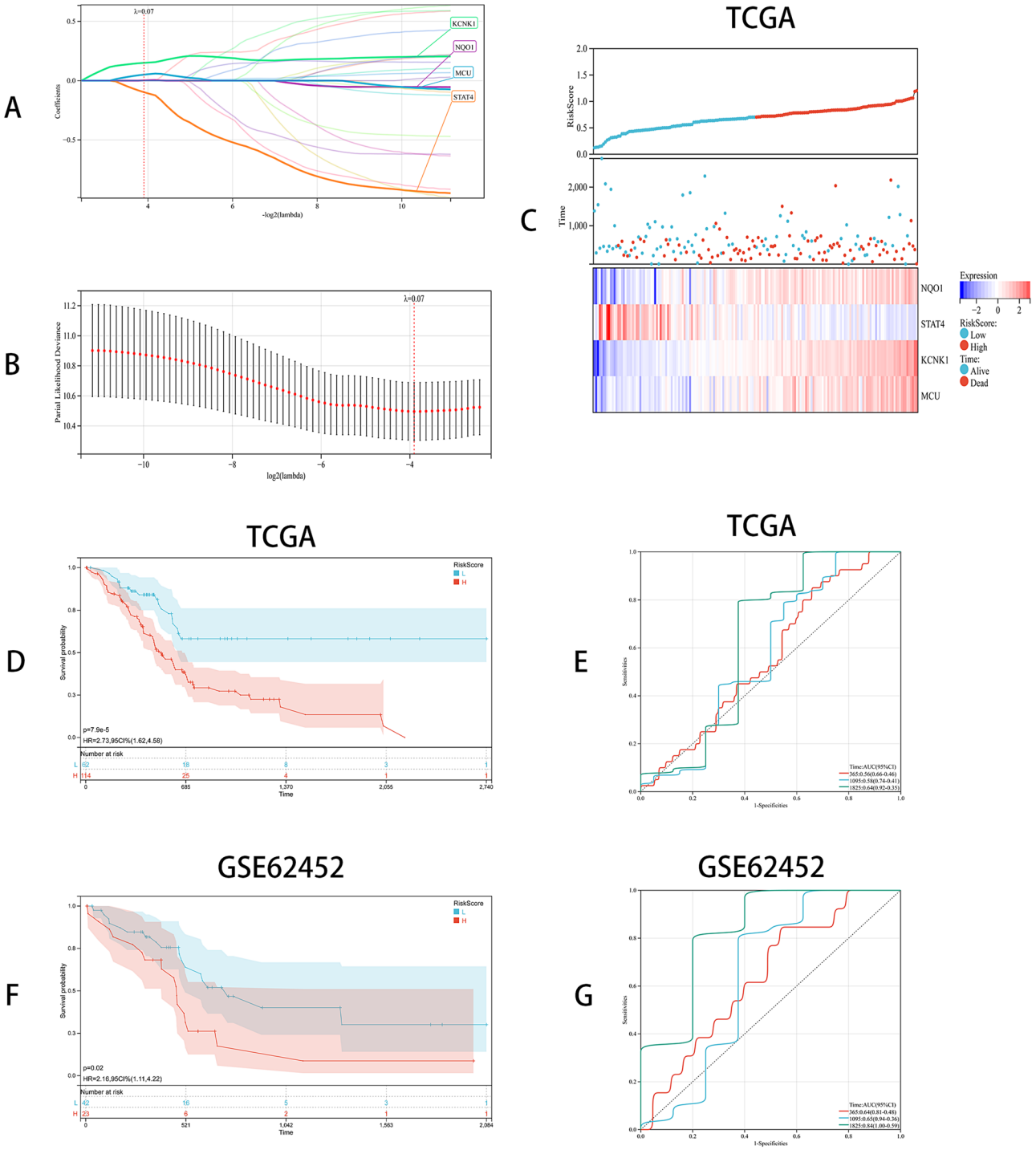

Fig. 5 Constructing and confirming the Lactate risk profile. (**A**-**B**) Lasso Cox regression evaluation; (**C**) Score allocation of SFRGs and patient outcome patterns in the TCGA dataset. (**D**-**E**) KM analysis and temporal ROC curve evaluation for risk stratification in the TCGA dataset. (**F**-**G**) Kaplan-Meier analysis and temporal ROC curve evaluation for risk stratification in the GSE62452 dataset

of 0.64 for the 1-year survival, 0.65 for the 3-year survival, and 0.84 for the 5-year survival (Fig. 5G).

Single cell analysis of LRGs

In our current research, We identified four LRGs associated with PDAC (KCNK1, MCU, NQO1 and STAT4). To delve deeper into the interplay between these LRG expressions and the tumor immune landscape, we utilized the TISCH. We analyzed 2 datasets that were PDAC_CRA001160 dataset and the PDAC_GSE162708 dataset (Fig. 6A-B). Within the PDAC_CRA001160 dataset, elevated levels of KCNK1 and MCU were observed in Malignant cells, while NQO1 showed high expression in both Malignant and Endothelial cells, and STAT4 exhibited strong expression in Plasma cells (Fig. 6C-F). Correspondingly, in the PDAC_GSE162708 dataset, KCNK1 demonstrated notable expression in Malignant cells, MCU displayed high levels in both Malignant and Endothelial cells, NQO1 displayed elevated expression in Endothelial cells, and STAT4 exhibited marked expression in NK cells and CD8 T cells as depicted in Fig. 6G-J.

Expression and prognosis of LRGs

To find the expression of these four LRGs in PDAC, we performed a search using GEPIA2.0. It was found that KCNK1, MCU, and NQO1 showed high expression in tumor tissues. Moreover, elevated MCU levels were notably linked to unfavorable clinical outcomes (Fig. 7A-H).

Multilevel expression validation and in vitro functional investigation of MCU

Given the high expression of MCU in pancreatic cancer patients and its prognostic relevance, we selected MCU for subsequent biological experiments. In order to verify the biological function of MCU, we conducted qRT-PCR (Fig. 8A) and WB (Fig. 8B) in whole pancreatic cancer cell lines and normal pancreatic epithelial cells and found that MCU was generally highly expressed in pancreatic cancer cell lines, especially in Bxpc3 and Capan1 cells. By verifying the knockdown efficiency of plasmids, it was found that sh1 and sh4 had the best knockdown effect (Fig. 8C-D). Therefore, we chose to use sh1 and sh4 plasmosomes to knock down MCU genes in Bxpc3 and Capan1 cells to observe whether altering MCU expression would affect the malignant potential of tumor cells. Colony-formation assay (Fig. 8E-F) and CCK8 experiments (Fig. 8G) revealed that MCU gene silencing resulted in decreased proliferation rates of pancreatic cancer cells, suggesting the MCU gene's role in enhancing pancreatic cancer cell proliferation. The impact of MCU suppression on cellular motility (Fig. 8H-I) and invasiveness (Fig. 8J-K) was evaluated using transwell assays, demonstrating reduced migration and invasion capabilities. Furthermore, the sphere-formation assay (Fig. 8L) examined how MCU downregulation influenced pancreatic cancer stemness, revealing diminished stem cell properties following reduced MCU expression. These experimental observations provide substantial evidence that MCU enhances pancreatic cancer cell proliferation, motility, invasiveness, and stemness characteristics, thereby contributing to the aggressive nature of pancreatic cancer. To further explore the metabolic implications of MCU in pancreatic cancer progression, we performed lactate quantification and NAD+/NADH ratio analysis in MCU-knockdown cells. Strikingly, both Bxpc3 and Capan1 cells with MCU silencing (sh1/sh4) exhibited significantly reduced intracellular lactate levels compared to NC controls (Supplementary Figure C), accompanied by a marked elevation in the NAD+/NADH ratio (Supplementary Figure A-B), indicative of attenuated glycolytic flux. Consistent with these findings, western blot analysis revealed downregulation of key glycolytic regulators (HK2, LDHA, and PDK1) upon MCU depletion (Supplementary Figure D-E). These data collectively demonstrate that MCU sustains the Warburg effect by promoting glycolysis-driven lactate production, while its suppression shifts cellular redox balance toward a more oxidized state (elevated NAD+/NADH). This metabolic reprogramming mechanism may underlie the observed impairment in proliferation, motility, and stemness properties, as tumor cells critically depend on glycolytic metabolism to fuel their aggressive phenotypes. Our findings thereby establish a novel functional link between MCU and cancer-associated metabolic reprogramming in pancreatic malignancy.

Discussion

PDAC is recognized as one of the most aggressive malignancies. It is characterized by early metastasis and late diagnosis, often presenting at advanced stages with limited treatment options [1]. Despite advancements in therapeutic strategies, including surgical resection, chemotherapy, and targeted therapies, the aggregate 5-year survival outcome remains unfavorable, primarily due to the high degree of chemoresistance and early metastatic spread inherent to PDAC [3, 4]. A significant bottleneck in enhancing patient results is the absence of effective predictive biomarkers that can guide treatment strategies and prognostication. Identifying such biomarkers is imperative, as they could potentially stratify patients for more tailored therapies, predict treatment response, and provide a valuable understanding of the intricate interactions between the TME and PDAC progression [15]. The advancement of computational biology software and the amalgamation of diverse -omics datasets have paved the way for identifying innovative biological indicators [16]. These advances are critical in the quest to understand the molecular underpinnings of PDAC and to identify

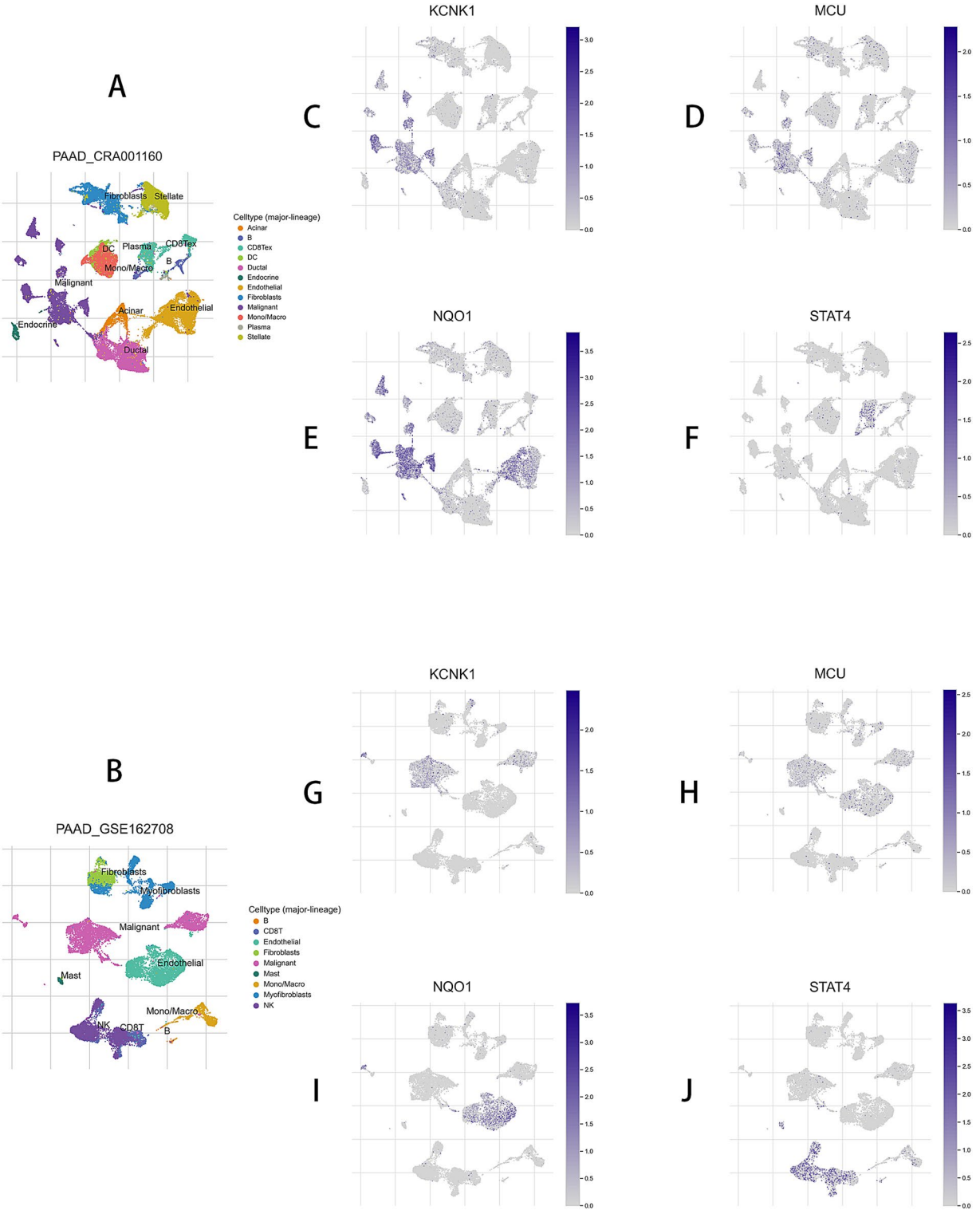

Fig. 6 Single cell analysis of LRGs in PDAC. (**A**-**J**) Cellular-level mapping unveiled the allocation of KCNK1, MCU, NQO1 and STAT4 across diverse immune cell populations in PDAC_CRA001160 and PDAC_GSE162708

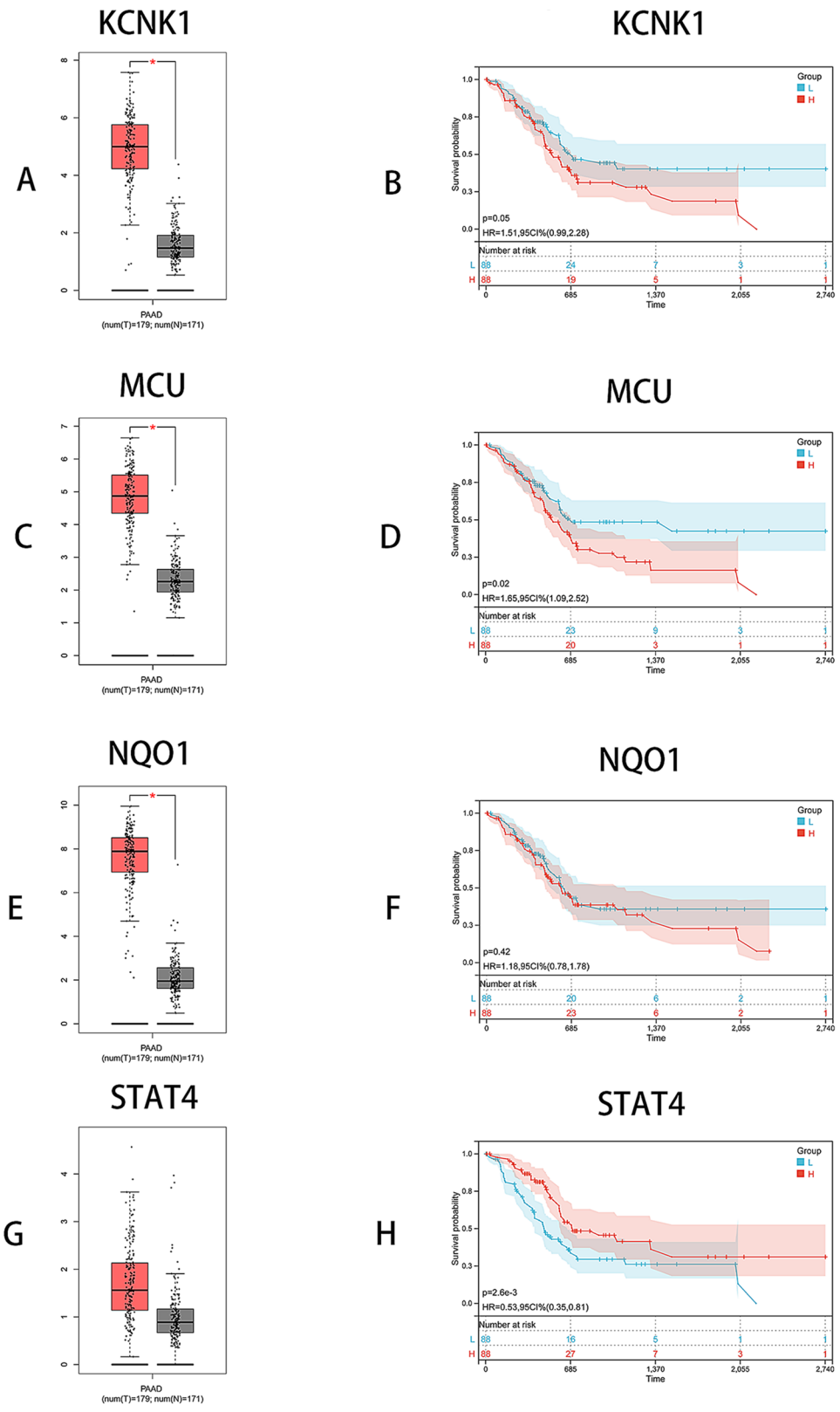

Fig. 7 The prognostic value and expression of LRGs. (**A**-**H**) Differential analysis of mRNA expression of KCNK1, MCU, NQO1 and STAT4 in PDAC in GEPIA2.0 database (Independent t-test). Kaplan–Meier curve for OS between the high and low expression cohort in PDAC in TCGA database (log-rank test).(* $P<0.05$)

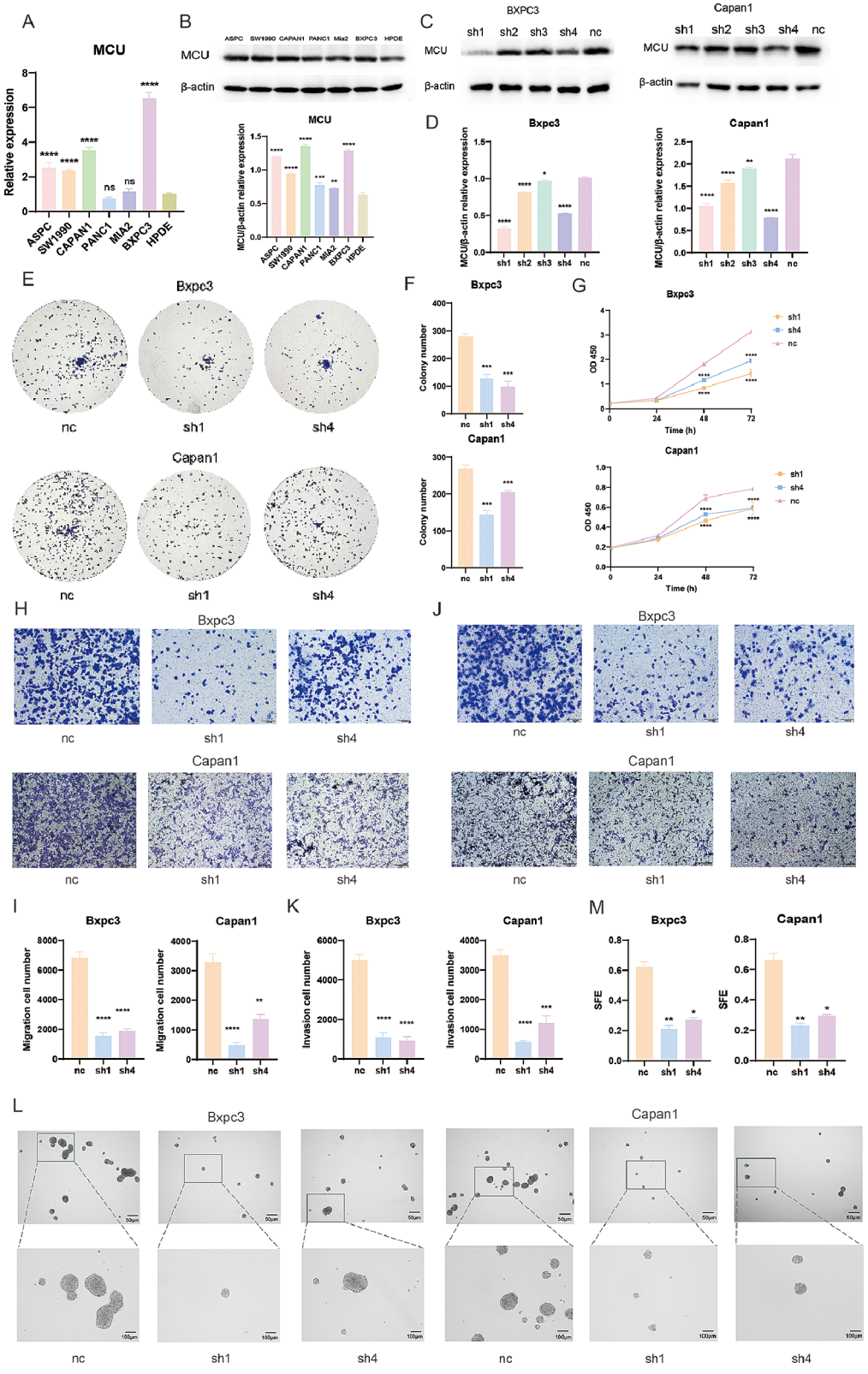

Fig. 8 (See legend on next page.)

(See figure on previous page.)

Fig. 8 Verification of MCU biological function. (**A**) qRT-PCR: Examining MCU expression patterns between pancreatic cancer cell lines and normal pancreatic epithelial cells (Kruskal-Wallis test); (**B**) WB: To verify the expression level of MCU and the quantitation of WB in pancreatic cancer cell lines and normal pancreatic epithelial cells (Kruskal-Wallis test); (**C**) WB: Knock-down efficiency of plasmid in Capan1 and Bxpc3 cells; (**D**) Knock-down quantification of WB to verify inefficiency (Kruskal-Wallis test); (**E**) Colony-formation assay after reducing MCU level in Capan1 and Bxpc3 cells; (**F**) Colony-formation assay quantification (Kruskal-Wallis test and Mann-Whitney U test, and Bonferroni); (**G**) CCK8 experiments after decreasing MCU level in Capan1 and Bxpc3 cells (One-way ANOVA and Dunnett test); (**H**) Transwell migration assay after decreasing MCU level in Capan1 and Bxpc3 cells; (**I**) Quantification of migration assay (One-way ANOVA and Dunnett test); (**J**) Transwell invasion assay after decreasing MCU expression in Capan1 and Bxpc3 cells; (**K**) Quantification of invasion assay (One-way ANOVA and Dunnett test); (**L**) Sphere-formation assay after reducing MCU expression in Capan1 and Bxpc3 cells (Kruskal-Wallis test and Mann-Whitney U test, and Bonferroni). (**M**) Quantitative and statistical analysis of Sphere-formation assay. (* $P<0.05$;** $P<0.01$;*** $P<0.001$;**** $P<0.0001$)

signatures that can predict treatment efficacy and patient survival [17].

The complexity of PDAC is further compounded by its intricate relationship with the immune system, where the TME can modulate immune responses to facilitate tumor growth and evade therapeutic interventions [5]. Lactate once considered a mere byproduct of glycolysis, is now recognized as a key mediator in cancer biology, particularly in PDAC, where it contributes to an acidic TME that impairs immune cell function and promotes macrophage polarization towards an immunosuppressive phenotype. Additionally, lactate acts as a signaling molecule, influencing pathways like GPR81 to modulate immune evasion and tumor growth, and it affects tumor angiogenesis by stabilizing HIFs [6–10]. The study of lactate in PDAC is of significant value as it provides a deeper understanding of the metabolic reprogramming that occurs in cancer cells. By elucidating the mechanisms through which lactate contributes to tumor progression, researchers can identify potential therapeutic targets that disrupt these processes. For instance, targeting lactate production or its signaling pathways could enhance the efficacy of existing cancer therapies by restoring immune surveillance and inhibiting tumor growth [18]. Moreover, elucidating the function of lactate in PDAC may contribute to establishing enhanced diagnostic methods and predictive indicators, enabling timely identification and improved treatment strategies for this condition [19].

Our study identifies two distinct lactate-associated subtypes of PDAC, characterized by unique gene expression profiles and divergent clinical outcomes. The creation of a risk signature model utilizing LRGs, particularly highlighting the involvement of *KCNK1*, *NQO1*, *STAT4* and *MCU*, offers a novel prognostic tool for PDAC patients. The high-risk cohort, as determined by the risk score, is linked to poorer survival rates, indicating the potential utility of this model in stratifying patients for more treatment approaches.

Prior studies have highlighted that KCNK1 is instrumental in driving the malignancy of tumor cells, particularly in terms of influencing the cell cycle and the aggressive growth and spread of cancer cells. KCNK1 is highly expressed in thyroid cancer, breast cancer (BRCA), non-functioning pituitary adenoma, PDAC and bladder cancer [20–24]. NQO1 is a two-electron reductase that is highly active in the pro-oxidative milieu of human malignancies, which makes it a selective marker for tumors [25]. The STAT4 gene, belonging to the STAT family, exhibits significant genetic variations that profoundly impact immune reactions and the progression of illnesses, particularly in the realms of cancer and autoimmune disorders. However, research outcomes display variability when examined across different studies and demographic groups [26–29]. MCU serves a critical function in cancer progression. It's upregulated in metastatic tumors, enhancing cellular movement and invasion through a ROS/HIF-1α molecular cascade. However, its effects vary across different cancer types and cell lines [30–32].In BRCA, particularly the triple-negative subtype, MCU expression links to tumor size and lymph node infiltration, and its downregulation reduces tumor size and cell motility in xenograft models [30]. In melanoma, MCU silencing suppresses cell proliferation while enhancing migratory and invasive capabilities, diminishing responsiveness to immune-based therapies [31]. In pancreatic cancer, MCU inhibition reduces HINT2-dependent apoptosis [33], MCU also drives the transfer and metabolic recovery of PDAC through a cysteine-dependent mechanism [34]. In colon cancer, miRNA-25 overexpression decreases $mtCa2+$ uptake and shows increased expression in human colon malignancies where MCU levels are diminished [35]. In hepatocellular carcinoma, MCU upregulation is associated with poor survival and metastasis, and its increase promotes ROS production and cell motility [36]. In ovarian cancer, MCU silencing diminishes cell proliferation and migration, which is linked to decreased ROS production [37]. In renal cell carcinoma, MCU expression reduction leads to decreased cell migration and metastatic potential [38]. Fibroblast cell transformation is associated with upregulation of MCU expression that results in altered mitochondrial Ca^{2+} uptake kinetics and suppression of inactivating-phosphorylation of PDH that was nevertheless not associated with enhanced pyruvate metabolism through PDH or OCR. Rather, transformation was associated with enhanced aerobic glycolysis and anaplerotic glutamine and glucose metabolism [39]. These studies highlight the diverse effects of MCU modulation in different cancers. In this study, we have validated that MCU promotes the proliferation, migration, invasion, and

stemness of tumor cells in pancreatic cancer, thereby confirming the malignant potential of the MCU gene in this disease. Meanwhile, it has also been proved that MCU can promote the process of lactic acid generation and glycolysis. This indicates that MCU might serve as a crucial factor in the immune regulation and malignant advancement of PDAC. The clinical application value of MCU in PDAC lies in its potential as a therapeutic target and a biomarker for prognosis and response to therapy.

Clinical strategies targeting mitochondrial calcium unidirectional transporters (MCU) mainly include small molecule inhibitors (such as the natural drug berberine), gene editing technology and precise delivery systems. Berberine inhibits calcium overload by blocking the MCu-emre complex and shows cardiac protective effects in myocardial ischemia models [40]. Due to its high safety and strong penetration, it has become the first candidate drug expected to enter clinical trials. However, traditional inhibitors (such as ruthenium red) are still limited to basic research due to toxicity issues. Gene editing techniques have been confirmed to regulate neuronal excitability in epilepsy models, suggesting their potential in neurological diseases [41]. Current research focuses on optimizing the pharmacokinetic properties of berberine and developing targeted delivery systems (such as nanoparticles) to enhance tissue specificity. However, MCU-targeted therapy still faces significant limitations: It is widely involved in normal metabolism, and long-term inhibition may cause mitochondrial dysfunction; The mechanism of action of MCU in different diseases is heterogeneous; In addition, the risk of drug resistance and the selection of indications need to be further verified. In the future, AI drug design and multi-model validation need to be combined to promote its clinical transformation.

The use of data from TCGA and GEO databases provided a robust foundation for our analysis. The application of WGCNA and consensus clustering allowed us to delineate distinct lactate subtypes, each with unique gene expression profiles and clinical implications. This methodological approach enabled us to identify differentially expressed genes and construct a lactate-linked risk signature with significant prognostic value. However, it is important to acknowledge the limitations of our study. The reliance on existing databases introduces inherent biases, including (1) patient heterogeneity arising from variations in age, ethnicity, and disease stage across collection sites, and (2) technical biases from differing sequencing platforms (e.g., RNA-seq vs. microarray) and batch effects that may confound cross-dataset comparisons. Additionally, while our in vitro experiments provided valuable insights into the function of MCU in PDAC cells, further validation through complementary approaches would strengthen these findings. Patient-derived organoid models could better recapitulate tumor microenvironment interactions, while CRISPR-based functional screens might systematically identify co-dependent pathways in MCU-mediated PDAC progression. Prospective validation in multicenter clinical cohorts and spatial transcriptomics analysis could further confirm the clinical translatability of our risk signature.

The identification of two lactate subtypes with distinct clinical outcomes highlights the potential for personalized treatment strategies in PDAC. *While existing classification models (e.g., Collisson molecular subtypes or Moffitt stromal subtypes)* [42, 43] *primarily focus on tumor differentiation or microenvironment features, our lactate-centric stratification uniquely captures metabolic reprogramming dynamics that complement current frameworks by identifying druggable vulnerabilities in energy metabolism pathways. Recent studies reveal that lactate accumulation in PDAC not only drives histone lactylation (e.g., H3K18la) to promote cell cycle progression genes (TTK and BUB1B) through a glycolysis-lactylation positive feedback loop* [44], *but also enhances chemotherapy resistance by upregulating DNA synthesis via the oxidative pentose phosphate pathway. Specifically, glycolytic flux through the GLUT1/ALDOB/G6PD axis in glucometabolic PDAC subtypes increases nucleotide precursor production* [45] *enabling tumor cells to counteract DNA damage induced by chemotherapy agents.* Building upon these metabolic dependencies, the four lactate-related genes (LRGs) in our signature were identified as critical regulators of the glycolysis-lactylation axis, whose coordinated expression patterns stratify patients based on their capacity to sustain chemoresistance-supporting nucleotide biosynthesis and cell cycle progression. The risk signature we developed, comprising four LRGs, offers a novel tool for prognostic assessment. This signature could be used to stratify patients into different risk groups, potentially guiding treatment decisions and improving patient outcomes. Specifically, high-risk patients exhibiting MCU-driven metabolic profiles might benefit from early intensification of therapy (e.g., modified FOLFIRINOX regimens) combined with mitochondrial calcium modulation, whereas low-risk subtypes could avoid overtreatment through de-escalation strategies. The role of MCU in PDAC malignancy, confirmed through our in vitro experiments, presents a promising therapeutic target. Future research should focus on validating these findings in larger cohorts and exploring the potential of targeting MCU and other LRGs in clinical trials. Integrating lactate subtype classification with emerging therapeutic algorithms (e.g., PARP inhibitor sensitivity predictors or immunotherapy response biomarkers) may further refine PDAC precision medicine paradigms. Notably, combining lactate-targeting

approaches (e.g., LDHA inhibitors) with ERK pathway blockers may overcome adaptive resistance mechanisms triggered by metabolic stress, as demonstrated in glutamine antagonism studies. Additionally, investigating the interplay between lactate metabolism, protein lactylation, and the immune response in PDAC could reveal new therapeutic avenues and biomarkers for early detection and treatment.

Conclusion

The research conducted on lactate-related genes (LRGs) in pancreatic ductal adenocarcinoma (PDAC) has shed light on their potential impact on tumor development, particularly through their influence on the tumor microenvironment and immune evasion mechanisms. The findings presented in this study have revealed the existence of distinct lactate subtypes in PDAC, each associated with unique gene expression patterns and clinical outcomes. Through the development of a predictive risk signature comprised of four LRGs, this investigation has not only provided valuable insights into the prognostic implications of lactate metabolism in PDAC but has also identified potential therapeutic targets for intervention. Additionally, the functional validation of the mitochondrial calcium uniporter (MCU) in PDAC cells has further emphasized the significance of LRGs in driving the malignancy of this aggressive cancer type. Overall, this study underscores the critical role of LRGs in PDAC pathogenesis and highlights the potential for novel prognostic tools and targeted therapies in the management of pancreatic cancer.

Abbreviations

ATCC	American Type Culture Collection
AUC	Area Under the Curve
BRCA	Breast Cancer Susceptibility Gene
BSA	Bovine Serum Albumin
Bxpc3	Biopsy xenograft of Pancreatic Carcinoma line-3
CAMs	Cell Adhesion Molecules
CCK8	Cell Counting Kit-8
CDF	Cumulative Distribution Function
DEGs	Differentially Expressed Genes
DMEM	Dulbecco's Modified Eagle's Medium
FBS	Fetal Bovine Serum
FDR	False Discovery Rate
GEO	Gene Expression Omnibus
GSEA	Gene Set Enrichment Analysis
HIFs	Hypoxia-Inducible Factors
HRP	Horseradish Peroxidase
KM	Kaplan-Meier
LRGs	Lactate-Related Genes
OS	Overall Survival
PBS	Phosphate Buffered Saline
PDAC	Pancreatic Ductal Adenocarcinoma
PFA	Paraformaldehyde
ROC	Receiver Operating Characteristic
ROS	Reactive Oxygen Species
RPMI-1640	Roswell Park Memorial Institute Medium 1640
TCGA	The Cancer Genome Atlas
Th17	T helper cell 17
TISCH	Tumor Immune Single Cell Center
TME	Tumor Microenvironment
WB	Western Blot

Supplementary Information

The online version contains supplementary material available at https://doi.org/10.1186/s12885-025-14319-1.

Supplementary Material 1

Supplementary Material 2

Supplementary Material 3

Supplementary Material 4

Supplementary Material 5

Supplementary Material 6

Supplementary Material 7

Supplementary Material 8

Acknowledgements

Not applicable.

Author contributions

Yuhang Chen: Writing–review&editing, Experiment, Methodology. Fenglin Zhang: Writing – original draft, Experiment. Suoyi Dai: Software. Jiangang Zhao and Wenxun Cai: Experiment. Ke Zhang: Writing – original draft, Data curation, Formal analysis. Xinghe Liao: Writing – review & editing, Validation. Lianyu Chen: Validation, Supervision.

Funding

This study was supported by the National Natural Science Foundation of China (82174169) and Fudan University DIGAOJIAN Project (No.DGF601020-1).

Data availability

The data examined in this research were derived from openly accessible databases: https://portal.gdc.cancer.gov/ (TCGA-PAAD) and the Gene Expression Omnibus (GEO) (https://www.ncbi.nlm.nih.gov/geo/).

Declarations

Ethics approval and consent to participate

Not applicable. All data in this study are publicly available.

Consent for publication

Not applicable.

Competing interests

The authors declare no competing interests.

Author details

[1]Department of Integrative Oncology, Fudan University Shanghai Cancer Center, Shanghai 200032, China
[2]Department of Oncology, Shanghai Medical College, Fudan University, Shanghai 200032, China
[3]Department of Integrated Therapy, Fudan University Shanghai Cancer Center, Shanghai 200032, China
[4]Department of Oncology, Shaoxing Central Hospital, Shaoxing 312030, China
[5]Department of Oncology, The Central Affiliated Hospital, Shaoxing University, Shaoxing 312030, China
[6]Oncology Department of Integrated Traditional Chinese and Western Medicine, The First Affiliated Hospital of Anhui Medical University, Hefei 230022, China
[7]Graduate School of Anhui, University of Traditional Chinese Medicine, Hefei 230022, China
[8]Shanghai Traditional Chinese Medicine Integrated Hospital, Shanghai University of Traditional Chinese Medicine, Shanghai 200082, China

Received: 25 January 2025 / Accepted: 13 May 2025
Published online: 21 May 2025

References

1. Siegel RL, Giaquinto AN, Jemal A. Cancer statistics, 2024. CA Cancer J Clin. 2024;74(1):12–49.
2. Rahib L, Smith BD, Aizenberg R, Rosenzweig AB, Fleshman JM, Matrisian LM. Projecting cancer incidence and deaths to 2030: the unexpected burden of thyroid, liver, and pancreas cancers in the united States. Cancer Res. 2014;74(11):2913–21.
3. Yu S, Zhang C, Xie KP. Therapeutic resistance of pancreatic cancer: roadmap to its reversal. Biochim Biophys Acta Rev Cancer. 2021;1875(1):188461.
4. Grossberg AJ, Chu LC, Deig CR, et al. Multidisciplinary standards of care and recent progress in pancreatic ductal adenocarcinoma. CA Cancer J Clin. 2020;70(5):375–403.
5. Hu ZI, O'Reilly EM. Therapeutic developments in pancreatic cancer. Nat Rev Gastroenterol Hepatol. 2024;21(1):7–24.
6. Warburg O, Wind F, Negelein E. The metabolism of tumors in the body. J Gen Physiol. 1927;8(6):519–30.
7. Quinn WJ 3rd, Jiao J, TeSlaa T, et al. Lactate limits T cell proliferation via the NAD(H) redox state. Cell Rep. 2020;33(11):108500.
8. Colegio OR, Chu NQ, Szabo AL, et al. Functional polarization of tumour-associated macrophages by tumour-derived lactic acid. Nature. 2014;513(7519):559–63.
9. Brown TP, Ganapathy V. Lactate/GPR81 signaling and proton motive force in cancer: role in angiogenesis, immune escape, nutrition, and Warburg phenomenon. Pharmacol Ther. 2020;206:107451.
10. Hui S, Ghergurovich JM, Morscher RJ, et al. Glucose feeds the TCA cycle via Circulating lactate. Nature. 2017;551(7678):115–8.
11. Semenza GL. Hypoxia-inducible factors in physiology and medicine. Cell. 2012;148(3):399–408.
12. Zhang D, Tang Z, Huang H, et al. Metabolic regulation of gene expression by histone lactylation. Nature. 2019;574(7779):575–80.
13. Dai E, Wang W, Li Y, Ye D, Li Y. Lactate and lactylation: behind the development of tumors. Cancer Lett. 2024;591:216896.
14. Jiang K, Zhu L, Huang H, Zheng L, Wang Z, Kang X. Lactate score classification of hepatocellular carcinoma helps identify patients with tumors that respond to immune checkpoint Blockade therapy. Cell Oncol (Dordr). 2024;47(1):175–88.
15. Bailey P, Chang DK, Nones K, et al. Genomic analyses identify molecular subtypes of pancreatic cancer. Nature. 2016;531(7592):47–52.
16. Hoadley KA, Yau C, Wolf DM, et al. Multiplatform analysis of 12 cancer types reveals molecular classification within and across tissues of origin. Cell. 2014;158(4):929–44.
17. Collisson EA, Sadanandam A, Olson P, et al. Subtypes of pancreatic ductal adenocarcinoma and their differing responses to therapy. Nat Med. 2011;17(4):500–3.
18. Ippolito L, Morandi A, Giannoni E, Chiarugi P. Lactate: A metabolic driver in the tumour landscape. Trends Biochem Sci. 2019;44(2):153–66.
19. Li X, Yang Y, Zhang B, et al. Lactate metabolism in human health and disease [published correction appears in. Signal Transduct Target Ther. 2022;7(1):372.
20. Lin X, Wu JF, Wang DM, Zhang J, Zhang WJ, Xue G. The correlation and role analysis of KCNK2/4/5/15 in human papillary thyroid carcinoma microenvironment. J Cancer. 2020;11(17):5162–76.
21. Huang X, Feng Y, Ma D, et al. The molecular, immune features, and risk score construction of intraductal papillary mucinous neoplasm patients. Front Mol Biosci. 2022;9:887887.
22. Karatug Kacar A, Bulutay P, Aylar D, Celikten M, Bolkent S. Characterization and comparison of Insulinoma tumor model and pancreatic damage caused by the tumor, and identification of possible markers. Mol Biol Rep. 2024;51(1):109.
23. Xiong F, Wu GH, Wang B, Chen YJ. Plastin-3 is a diagnostic and prognostic marker for pancreatic adenocarcinoma and distinguishes from diffuse large B-cell lymphoma. Cancer Cell Int. 2021;21(1):411.
24. Zhang W, Chen XS, Wei Y, et al. Overexpressed KCNK1 regulates potassium channels affecting molecular mechanisms and biological pathways in bladder cancer. Eur J Med Res. 2024;29(1):257.
25. Khan AEMA, Arutla V, Srivenugopal KS. Human NQO1 as a selective target for anticancer therapeutics and tumor imaging. Cells. 2024;13(15):1272.
26. Wang C, Gao N, Yang L, et al. Stat4 rs7574865 polymorphism promotes the occurrence and progression of hepatocellular carcinoma via the Stat4/CYP2E1/FGL2 pathway. Cell Death Dis. 2022;13(2):130.
27. Ma Y, Zhou Y, Zhang H, Su X. Immune Response-Related Genes - STAT4, IL8RA and CCR7 polymorphisms in lung cancer: A Case-Control study in China. Pharmgenomics Pers Med. 2020;13:511–9.
28. Cotterchio M, Lowcock E, Bider-Canfield Z, et al. Association between variants in Atopy-Related Immunologic candidate genes and pancreatic Cancer risk. PLoS ONE. 2015;10(5):e0125273.
29. Núñez-Marrero A, Arroyo N, Godoy L, Rahman MZ, Matta JL, Dutil J. SNPs in the interleukin-12 signaling pathway are associated with breast cancer risk in Puerto Rican women. Oncotarget. 2020;11(37):3420–31.
30. Tosatto A, Sommaggio R, Kummerow C, et al. The mitochondrial calcium uniporter regulates breast cancer progression via HIF-1α. EMBO Mol Med. 2016;8(5):569–85.
31. Stejerean-Todoran I, Zimmermann K, Gibhardt CS, et al. MCU controls melanoma progression through a redox-controlled phenotype switch. EMBO Rep. 2022;23(11):e54746.
32. Vultur A, Gibhardt CS, Stanisz H, Bogeski I. The role of the mitochondrial calcium uniporter (MCU) complex in cancer. Pflugers Arch. 2018;470(8):1149–63.
33. Chen L, Sun Q, Zhou D, et al. HINT2 triggers mitochondrial Ca2 + influx by regulating the mitochondrial Ca2 + uniporter (MCU) complex and enhances gemcitabine apoptotic effect in pancreatic cancer. Cancer Lett. 2017;411:106–16.
34. Wang X, Li Y, Li Z, et al. Mitochondrial calcium uniporter drives metastasis and confers a targetable cystine dependency in pancreatic Cancer. Cancer Res. 2022;82(12):2254–68.
35. Marchi S, Lupini L, Patergnani S, et al. Downregulation of the mitochondrial calcium uniporter by cancer-related miR-25. Curr Biol. 2013;23(1):58–63.
36. Ren T, Zhang H, Wang J, et al. MCU-dependent mitochondrial Ca2 + inhibits NAD+/SIRT3/SOD2 pathway to promote ROS production and metastasis of HCC cells. Oncogene. 2017;36(42):5897–909.
37. Zhao L, Jiang M, Tian T, et al. Effects of MCU-mediated Ca2 + Homeostasis on ovarian Cancer cell SKOV3 proliferation, migration and transformation. Curr Mol Med. 2023;23(8):774–83.
38. Meng K, Hu Y, Wang D, et al. EFHD1, a novel mitochondrial regulator of tumor metastasis in clear cell renal cell carcinoma. Cancer Sci. 2023;114(5):2029–40.
39. Fernandez Garcia E, Paudel U, Noji MC, et al. The mitochondrial Ca^{2+} channel MCU is critical for tumor growth by supporting cell cycle progression and proliferation. Front Cell Dev Biol. 2023;11:1082213.
40. Zhao H, Chen S, Cao N, et al. Berberine is a novel mitochondrial calcium uniporter inhibitor that disrupts MCU-EMRE assembly. Adv Sci (Weinh) Published Online Febr. 2025;7. https://doi.org/10.1002/advs.202412311.
41. Bierhansl L, et al. Neuronal mitochondrial calcium uniporter (MCU) deficiency is neuroprotective in hyperexcitability by modulation of metabolic pathways and ROS balance. Mol Neurobiol Vol. 2024;61:9529–38. https://doi.org/10.1007/s12035-024-04148-x.
42. Martinez-Useros J, Martin-Galan M, Garcia-Foncillas J. The match between molecular subtypes, histology and microenvironment of pancreatic Cancer and its relevance for chemoresistance. Cancers (Basel). 2021;13(2):322. https://doi.org/10.3390/cancers13020322. Published 2021 Jan 17.
43. Biankin AV, Maitra A. Subtyping pancreatic Cancer. Cancer Cell. 2015;28(4):411–3. https://doi.org/10.1016/j.ccell.2015.09.020.
44. Li F, Si W, Xia L, et al. Positive feedback regulation between Glycolysis and histone lactylation drives oncogenesis in pancreatic ductal adenocarcinoma. Mol Cancer. 2024;23(1):90. https://doi.org/10.1186/s12943-024-02008-9. Published 2024 May 6.
45. Li Y, Tang S, Shi X, et al. Metabolic classification suggests the GLUT1/ALDOB/G6PD axis as a therapeutic target in chemotherapy-resistant pancreatic cancer. Cell Rep Med. 2023;4(9):101162. https://doi.org/10.1016/j.xcrm.2023.101162.

Publisher's note